Cell Metabolism

Article

Creatine promotes cancer metastasis through activation of Smad2/3

Graphical abstract

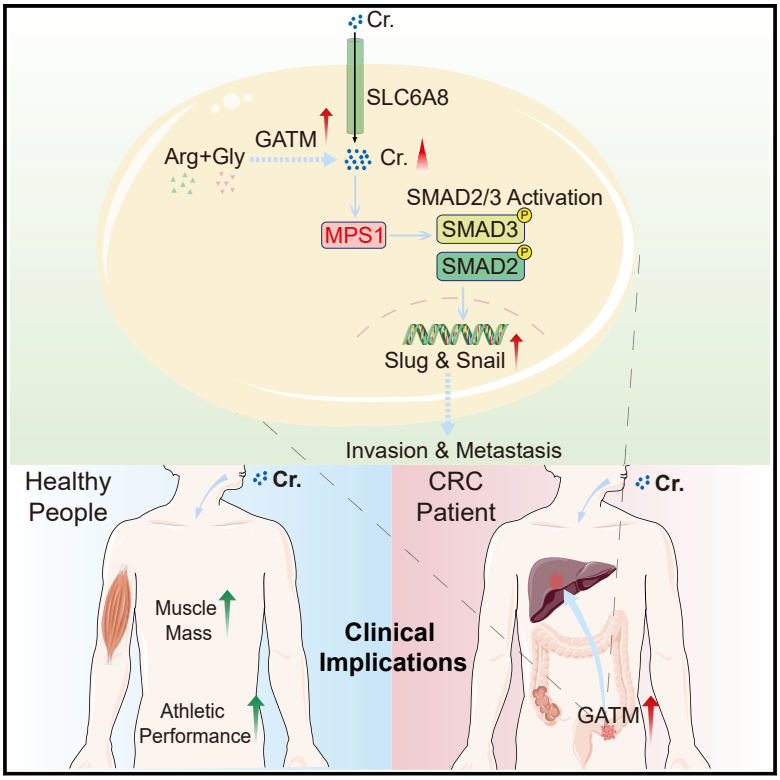

Highlights

- Dietary uptake of creatine promotes colorectal and breast cancer metastasis in mice
- GATM-mediated *de novo* synthesis of creatine enhances cancer metastasis
- Creatine promotes cancer metastasis through MPS1-activated Smad2 and Smad3
- Targeting GATM or MPS1 prevents colorectal and breast cancer metastasis in mice

Authors

Liwen Zhang, Zijing Zhu, Huiwen Yan, ..., Hai-long Piao, Gang Chen, Pengcheng Bu

Correspondence

hpiao@dicp.ac.cn (H.-l.P.), chendoctor@sina.com (G.C.), bupc@ibp.ac.cn (P.B.)

In brief

Creatine is widely used to improve muscle mass and function of healthy people. However, Zhang et al. report that creatine supplementation or high levels of endogenously synthesized creatine promote cancer metastasis in orthotopic mouse models of CRC and breast cancer by activating Smad2/3 through MPS1. Targeting creatine synthesis or MPS1 prevents the creatine-mediated cancer metastasis.

Zhang et al., 2021, Cell Metabolism *33*, 1–13
May 4, 2021
https://doi.org/10.1016/j.cmet.2021.03.009

CellPress

Cell Metabolism

CellPress

Article

Creatine promotes cancer metastasis through activation of Smad2/3

Liwen Zhang,[1,2] Zijing Zhu,[1,2] Huiwen Yan,[1] Wen Wang,[3] Zhenzhen Wu,[1] Fei Zhang,[1,2] Qixiang Zhang,[2,4] Guizhi Shi,[5] Junfeng Du,[6,7,8] Huiyun Cai,[6] Xuanxuan Zhang,[1,2] David Hsu,[9] Pu Gao,[2,4] Hai-long Piao,[3,*] Gang Chen,[6,*] and Pengcheng Bu[1,2,10,11,*]

[1]Key Laboratory of RNA Biology, Key Laboratory of Protein and Peptide Pharmaceutical, Institute of Biophysics, Chinese Academy of Sciences, Beijing 100101, China
[2]College of Life Sciences, University of Chinese Academy of Sciences, Beijing 100049, China
[3]CAS Key Laboratory of Separation Science for Analytical Chemistry, Dalian Institute of Chemical Physics, Chinese Academy of Sciences, Dalian 116023, China
[4]Key Laboratory of Infection and Immunity, Institute of Biophysics, Chinese Academy of Sciences, Beijing 100101, China
[5]Laboratory Animal Research Center, Institute of Biophysics, Chinese Academy of Sciences, Beijing 100101, China
[6]Department of General Surgery, the 7th Medical Center, Chinese PLA General Hospital, Beijing 100700, China
[7]The 2nd School of Clinical Medicine, Southern Medical University, Guangdong 510515, China
[8]Medical Department of General Surgery, the 1st Medical Center, Chinese PLA General Hospital, Beijing 100853, China
[9]Department of Medicine, Duke University School of Medicine, Durham 27708, USA
[10]Center for Excellence in Biomacromolecules, Chinese Academy of Sciences, Beijing 100101, China
[11]Lead contact
*Correspondence: hpiao@dicp.ac.cn (H.-l.P.), chendoctor@sina.com (G.C.), bupc@ibp.ac.cn (P.B.)
https://doi.org/10.1016/j.cmet.2021.03.009

SUMMARY

As one of the most popular nutrient supplements, creatine has been highly used to increase muscle mass and improve exercise performance. Here, we report an adverse effect of creatine using orthotopic mouse models, showing that creatine promotes colorectal and breast cancer metastasis and shortens mouse survival. We show that glycine amidinotransferase (GATM), the rate-limiting enzyme for creatine synthesis, is upregulated in liver metastases. Dietary uptake, or GATM-mediated *de novo* synthesis of creatine, enhances cancer metastasis and shortens mouse survival by upregulation of Snail and Slug expression via monopolar spindle 1 (MPS1)-activated Smad2 and Smad3 phosphorylation. GATM knockdown or MPS1 inhibition suppresses cancer metastasis and benefits mouse survival by downregulating Snail and Slug. Our findings call for using caution when considering dietary creatine to improve muscle mass or treat diseases and suggest that targeting GATM or MPS1 prevents cancer metastasis, especially metastasis of transforming growth factor beta receptor mutant colorectal cancers.

INTRODUCTION

Metastasis is the major cause of cancer-related death, accounting for approximately 90% of cancer-related mortality (Guan, 2015). Colorectal cancer (CRC) is the third leading cause of death and fourth most common diagnosed cancer (Rawla et al., 2019). Ten percent to 35% of patients with CRC present with metastasis at diagnosis and 70% of patients with CRC eventually develop liver metastasis (Bu et al., 2018; Zacharakis et al., 2010); most patients with CRC liver metastasis pass away in 6–20 months without treatment (Kulaylat and Gibbs, 2010). Even when treated with chemotherapy or managed by surgery, only 10% of patients survive for more than 5 years (Dueland et al., 2015). The challenge of effective CRC therapy is largely caused by our limited understanding of the mechanisms of CRC metastasis, which is often inconsistent with primary tumor growth.

Creatine, one of the most popular nutrient supplements, has been highly used to enhance the muscle mass and function of heathy human subjects, especially for athletes and body builders (Persky and Brazeau, 2001). Dietary creatine supplementation has even been used in clinical trials to reverse cachexia of patients with CRC, although the results demonstrated that creatine uptake failed to improve either muscle function or life quality of the patients (Norman et al., 2006). In addition, studies using subcutaneous injection mouse models showed that creatine uptake suppresses tumor growth, setting creatine as an anti-tumor supplement (Di Biase et al., 2019; Kristensen et al., 1999; Miller et al., 1993). However, subcutaneous injection mouse models are not clinically relevant for investigation of tumor progression, and tumor growth is not always coupled with metastasis (Ireson et al., 2019). Thus, it remains to be elucidated how creatine affects tumor progression, such as metastasis and patient survival.

Please cite this article in press as: Zhang et al., Creatine promotes cancer metastasis through activation of Smad2/3, Cell Metabolism (2021), https://doi.org/10.1016/j.cmet.2021.03.009

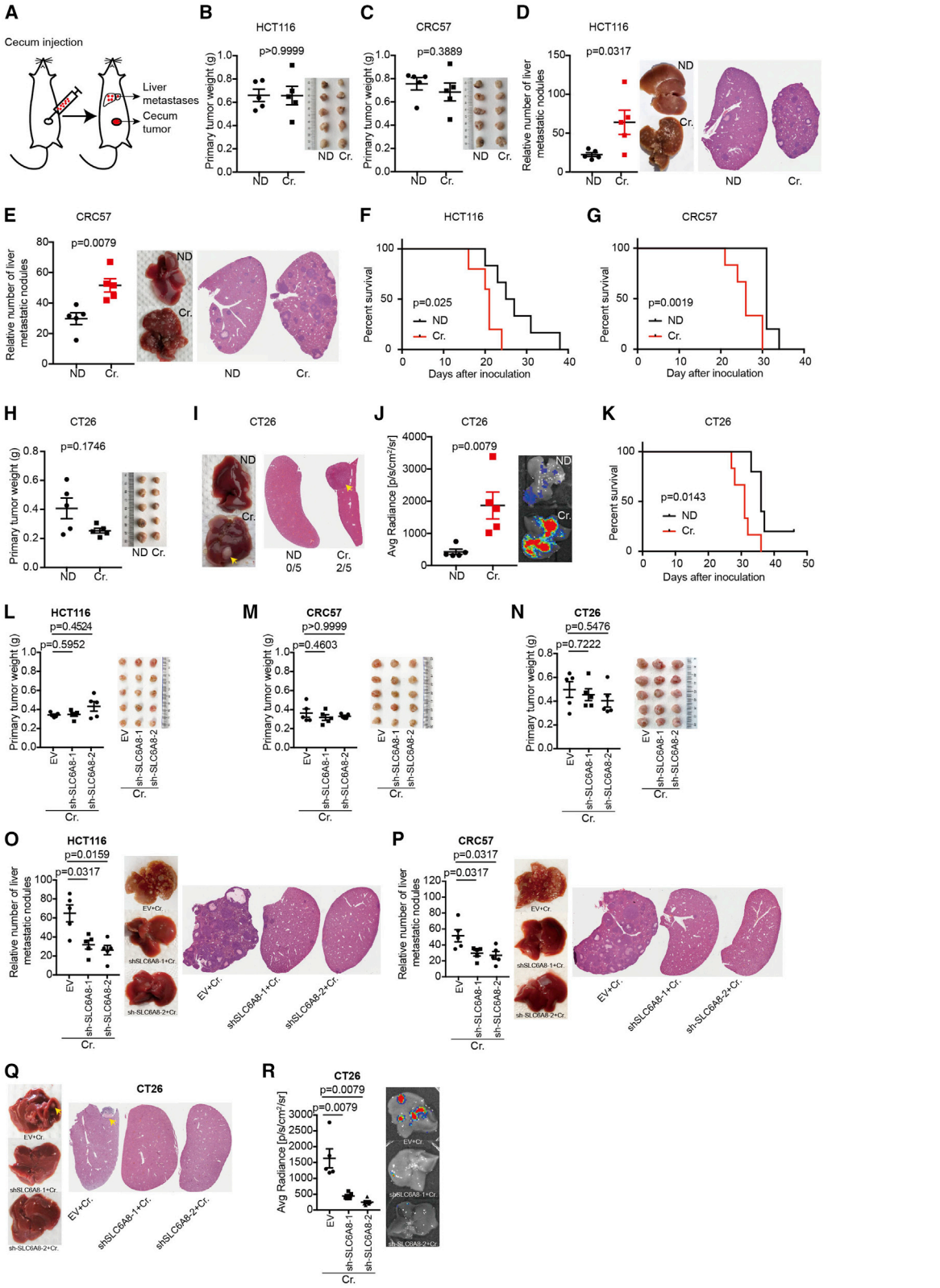

(legend on next page)

Please cite this article in press as: Zhang et al., Creatine promotes cancer metastasis through activation of Smad2/3, Cell Metabolism (2021), https://doi.org/10.1016/j.cmet.2021.03.009

RESULTS

Creatine promotes tumor metastasis

To investigate how creatine affects tumor metastasis, we used a CRC orthotopic mouse model by injecting a well-used CRC cell line HCT116 and a patient-derived xenograft (PDX) cell line CRC57 into cecum termini of NSG mice (Bu et al., 2015, 2018; Fu et al., 1991) (Figure 1A). One week after cecum injection, the mice were switched to a 5% w/w creatine supplemented diet or creatine-containing water (42.5 mg/mL, 400 μL/time, 3 times per week, a dose resembling that of human supplements) via oral gavage, whereas the control mice were kept on a regular diet. Once one mouse became moribund, all mice were simultaneously sacrificed for examination of primary tumor growth and liver metastasis. The CRC orthotopic mouse model showed that creatine either did not affect or slightly suppressed primary tumor growth in the cecum (Figures 1B, 1C, S1A, and S1B). However, creatine uptake significantly enhanced liver metastasis (Figures 1D, 1E, S1C, and S1D). We then set up another orthotopic mouse model by injecting HCT116 and CRC57 cells to investigate how creatine affects tumor-bearing mice survival. Consistent with the observation that creatine promoted CRC liver metastasis, we observed that creatine uptake significantly shortened survival time of the mice bearing either HCT116 or CRC57 cell-formed tumors (Figures 1F and 1G).

We then implanted a mouse CRC cell line CT26 into the cecum termini of BALB/c mice. As with HTC116 and CRC57 cells, the mice were switched to a 5% w/w creatine supplemented diet or creatine-containing water (42.5 mg/mL, 400 μL/time, 3 times per week) via oral gavage, and all mice were simultaneously sacrificed once one became moribund. Creatine-treated BALB/c mice harbored smaller primary tumors in the cecum (Figures 1H and S1E); however, creatine uptake promoted CT26 cells to metastasize to the liver, with 2 of 5 creatine diet-treated mice and 1 of 5 creatine-containing water-treated mice. In contrast, none of the control mice developed visible liver metastasis (Figures 1I and S1F). To examine the potential invisible live metastasis, we infected a luciferase-expressing construct into CT26 cells and injected the cells into the cecum termini of BALB/c mice. IVIS bioluminescence imaging showed that creatine-treated mice developed many more liver micro-metastases than the control mice (Figures 1J and S1G). In addition, creatine treatment significantly reduced survival time of tumor-bearing BALB/c mice (Figure 1K).

To examine whether creatine affects the metastasis of other tumors such as breast cancer, we injected a mouse breast cancer cell line 4T1 into the mammary fat pad of BALB/c mice (Figure S1H). Creatine treatment inhibited breast tumor growth in the fad pad (Figures S1I and S1J), while potently enhancing 4T1 cells to metastasize to the lungs (Figures S1K and S1L). In addition, creatine shortened the mouse survival (Figure S1M). Thus, dietary uptake of creatine also promotes breast cancer metastasis and shortens survival.

To investigate whether tumor cells from creatine-treated mice accumulate more creatine, we collected primary tumors and metastases from the mice orthotopically injected with HCT116, CRC57, and 4T1 cells and immediately measured creatine levels using capillary electrophoresis-mass spectrometry (CE-MS). We observed that the primary tumors and metastases from the creatine-treated mice contained much higher creatine levels than those from the control mice (Figures S1N–S1P). The control mice injected with CT26 cells did not develop visible liver metastasis; therefore, we measured creatine levels in the primary tumors, finding that creatine treatment significantly increased the creatine levels in the primary tumors (Figure S1Q). Furthermore, we knocked down creatine transporter SLC6A8 in HCT116, CRC57, CT26, and 4T1 cells (Figure S1R); subsequently injected the cells into mice orthotopically; and supplied with a creatine-containing diet. We observed that creatine supplement failed

Figure 1. Creatine promotes tumor metastasis

(A) Schematic of the CRC orthotopic mouse model. CRC cells were initially injected into mouse cecum wall and metastasized to liver.

(B and C) Representative bright-field images and quantification of tumor weight of primary CRC growth in NSG mice with cecum injection of HCT116 (B) and CRC57 cells (C) and fed with normal diet (ND) or creatine-supplemented diet (Cr.). Error bars denote mean ± SEM of five mice per group. p value was calculated based on Mann-Whitney test.

(D and E) Representative bright-field images, H&E, and quantification of CRC liver metastasis in NSG mice with cecum injection of HCT116 (D) and CRC57 cells (E) and fed with normal diet (ND) or creatine-supplemented diet (Cr.). Error bars denote mean ± SEM of five mice per group. p value was calculated based on Mann-Whitney test.

(F and G) Survival curve analysis of NSG mice with cecum injection of HCT116 (F) and CRC57 cells (G) and fed with normal diet (ND) or creatine-supplemented diet (Cr.) (5–6 mice per group). p value was calculated based on log-rank test.

(H) Representative bright-field images and quantification of tumor weight of primary CRC growth in BALB/c mice with cecum injection of CT26 cells and fed with normal diet (ND) or creatine-supplemented diet (Cr.). Error bars denote mean ± SEM of five mice per group. p value was calculated based on Mann-Whitney test.

(I and J) Representative bright-field images, H&E, IVIS luciferase images, and quantification of CRC liver metastasis in BALB/c mice with cecum injection of CT26 cells and fed with normal diet (ND) or creatine-supplemented diet (Cr.). Yellow arrows indicate metastatic tumor. Error bars denote mean ± SEM of five mice per group. p value was calculated based on Mann-Whitney test.

(K) Survival curve analysis of BALB/c mice with cecum injection of CT26 cells and fed with normal diet (ND) or creatine-supplemented diet (Cr.) (6 mice per group). p value was calculated based on log-rank test.

(L–N) Representative bright-field images and quantification of tumor weight of primary CRC growth in mice with cecum injection of HCT116 (L), CRC57 (M), and CT26 cells (N) with control (EV) vector or SLC6A8 knockdown (shSLC6A8-1 and shSLC6A8-2). Error bars denote mean ± SEM of five mice per group. p value was calculated based on Mann-Whitney test.

(O and P) Representative bright-field images, H&E, and quantification of CRC liver metastasis in NSG mice with cecum injection of HCT116 (O) and CRC57 cells (P) with control (EV) vector or SLC6A8 knockdown (shSLC6A8-1 and shSLC6A8-2). Error bars denote mean ± SEM of five mice per group. p value was calculated based on Mann-Whitney test.

(Q and R) Representative bright-field images, H&E, IVIS luciferase images, and quantification of CRC liver metastasis in BALB/c mice with cecum injection of CT26 cells with control (EV) vector or SLC6A8 knockdown (shSLC6A8-1 and shSLC6A8-2). Yellow arrows indicate metastatic tumor. Error bars denote mean ± SEM of five mice per group. p value was calculated based on Mann-Whitney test.

Please cite this article in press as: Zhang et al., Creatine promotes cancer metastasis through activation of Smad2/3, Cell Metabolism (2021), https://doi.org/10.1016/j.cmet.2021.03.009

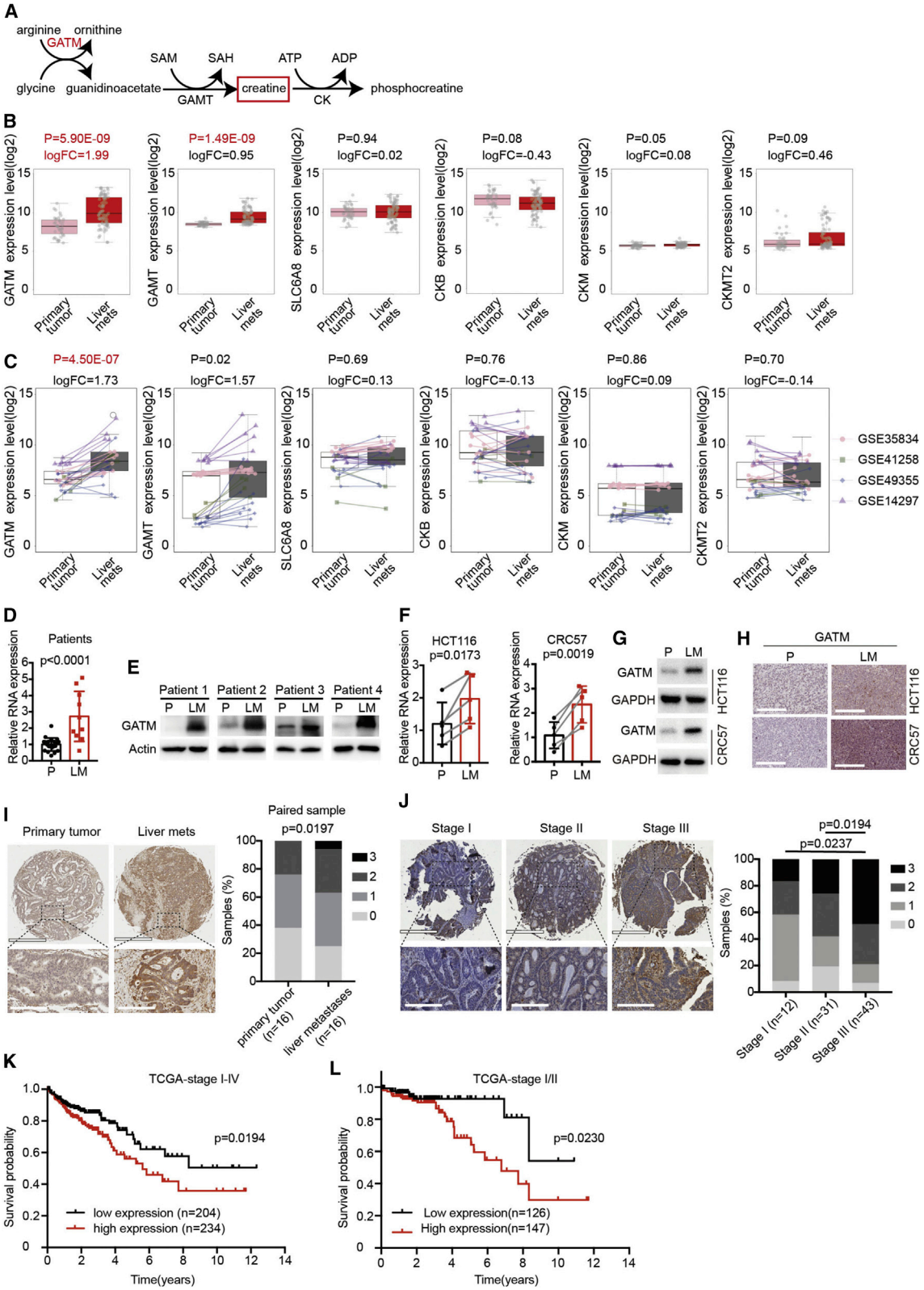

(legend on next page)

Please cite this article in press as: Zhang et al., Creatine promotes cancer metastasis through activation of Smad2/3, Cell Metabolism (2021), https://doi.org/10.1016/j.cmet.2021.03.009

to promote metastasis when SLC6A8 was knocked down in the cells (Figures 1L–1R, S1S, and S1T). Together, the data show that CRC and breast cancer cells take creatine from a dietary diet, promoting metastasis.

GATM is upregulated in CRC liver metastases

Creatine can be absorbed from the diet or synthesized through a two-step enzymatic reaction involving glycine amidinotransferase (GATM) and guanidinoacetate N-methyltransferase (GAMT). GATM catalyzes the rate-limiting step in creatine synthesis by transferring the amidino group of arginine to glycine to yield guanidinoacetic acid (GAA). GAA is then methylated by GAMT to generate creatine (Figure 2A). Creatine circulates in the blood and is siphoned into creatine-demanding tissue mediated by creatine transporter SLC6A8. Creatine kinase (CK) converts creatine into phosphorylcreatine, acting as an energy buffer (Wyss and Kaddurah-Daouk, 2000).

We analyzed the expression of GATM, GAMT, SLC6A8, and CK isoenzymes including CKMT2, CKM, and CKB from our previous microarray dataset that contains 39 primary colon carcinomas and 74 liver metastasis samples from patients with stage IV CRC (GEO: GSE41568) (Table S1). Gene expression analysis showed that GATM (log FC = 1.99) and GAMT (log FC = 0.95) were upregulated in the liver metastases compared with the primary tumors, whereas CKMT2, CKM, CKB, and SLC6A8 remained unchanged (Figure 2B). We further analyzed four NCBI Gene Expression Omnibus (GEO) datasets (GEO: GSE35834, GSE41258, GSE49355, and GSE14297) that contain transcriptomic profiling of 58 paired primary CRCs and liver metastases from 29 patients (Table S1). Integrated paired differential analysis further confirmed that GATM was significantly upregulated in liver metastasis (Figure 2C). In addition to CRCs, GATM expression is upregulated in metastases of other cancers such as breast cancer, melanoma, and neuroendocrine cancers (Figure S2A).

To further confirm GATM upregulation in CRC liver metastasis, we measured GATM expression in 21 primary CRC tumors and 10 CRC liver metastases collected from the 7th medical center of the PLA General Hospital (Table S2). Quantitative real-time PCR showed that GATM was indeed upregulated in CRC liver metastasis (Figure 2D). Western blot further confirmed GATM was consistently upregulated in the CRC liver metastasis compared with the paired primary CRC tumors (Figure 2E). We then performed cecum injection using mCherry-labeled HTC116 cells or GFP-labeled CRC57 cells, finding that liver metastases had significantly higher GATM expression than the primary tumor cells (Figures 2F–2H). Consistent with elevated GATM, liver metastatic cells contained higher levels of GAA and creatine than the primary tumor cells (Figures S2B and S2C).

GATM promotes CRC liver metastasis and targeting GATM prolongs mouse survival

To investigate whether GATM expression is associated with CRC progression, we examined GATM expression by immunohistochemistry staining of two tumor microarrays (TMAs). One TMA contained 32 paired CRC primary tumor and liver metastasis from 16 patients (Figure 2I; Table S2), and the other contained 12 stage I, 31 stage II, and 43 stage III CRC samples (Figure 2J; Table S2). GATM expression was not only significantly upregulated in liver metastases compared with paired primary tumors (Figure 2I) but also showed a higher expression level in the late than the early stage of CRCs (Figure 2J). GATM expression level was also strongly associated with clinical outcome. Comparison of the 438 patients with CRC from the TCGA database with the tumor stage, from I to IV, showed that high GATM levels in CRCs significantly shortened the patient survival time compared with low levels of GATM in patients (Figure 2K). To investigate whether GATM is a potential prognostic marker in the early stage of patients with CRC, we

Figure 2. GATM is upregulated in CRC liver metastases

(A) Diagram of GATM in creatine metabolism.

(B) Analysis of the expression levels of GATM, GAMT, SLC6A8, CKB, CKM, and CKMT2 on the base of our previous microarray measurements that contain 39 primary CRC and 74 liver metastatic samples from patients with stage IV CRC (GSE41568). p values were calculated based on a linear model using Limma.

(C) Paired box plots comparing expression levels of GATM, GAMT, SLC6A8, CKB, CKM, and CKMT2 between paired samples of primary CRC and liver metastases from 29 patients in four GEO datasets. Dots refer to different samples, and lines connect the paired samples. Different colors refer to different datasets. p values were calculated based on a paired linear model using Limma.

(D) Quantitative real-time PCR showing GATM expression levels in primary tumors (P) and liver metastases (LMs) collected from 21 patients with CRC. Data represent the mean ± SD. p value was calculated based on two-tailed Student's t test.

(E) Western blots showing GATM expression levels in paired primary tumors (P) and liver metastases (LMs) collected from 4 patients.

(F) Quantitative real-time PCR showing GATM expression levels in primary CRC tumors and liver metastasis derived from cecum-injected-HCT116 and CRC57 cells. Dots refer to different samples, and lines connect the paired samples. Error bars denote mean ± SD of five mice per group. p value was calculated based on two-tailed paired Student's t test.

(G) Western blots showing GATM expression levels in primary CRC tumor and liver metastatic cells derived from mice orthotopically injected with HCT116 and CRC57 cells.

(H) Representative immunohistochemistry images for measuring GATM expression in primary CRC tumors and liver metastasis derived from mice orthotopically injected with HCT116 and CRC57 cells. Scale bar, 200 μm.

(I) Representative immunohistochemistry images and evaluation of GATM expression measured on a tissue microarray that contains 16 paired primary CRC tumors and liver metastases. p value was calculated based on two-tailed paired Student's t test. Upper scale bar, 900 μm; lower scale bar, 200 μm.

(J) Representative immunohistochemistry images and evaluation of GATM expression measured on a tissue microarray that contains different stage of CRC samples. Stage I, n = 12; Stage II, n = 31; Stage III, n = 43. p value was calculated based on two-tailed paired Student's t test. Upper scale bar, 500 μm; lower scale bar, 200 μm.

(K) Kaplan-Meier analysis of survival curve of patients with CRC from stage I to IV with low (n = 204) and high (n = 234) GATM levels characterized by TCGA database. p value was calculated based on log-rank test.

(L) Kaplan-Meier analysis of survival curve of patients with CRC in stage I/II with low (n = 126) and high (n = 147) GATM levels characterized by TCGA database. p value was calculated based on log-rank test.

Please cite this article in press as: Zhang et al., Creatine promotes cancer metastasis through activation of Smad2/3, Cell Metabolism (2021), https://doi.org/10.1016/j.cmet.2021.03.009

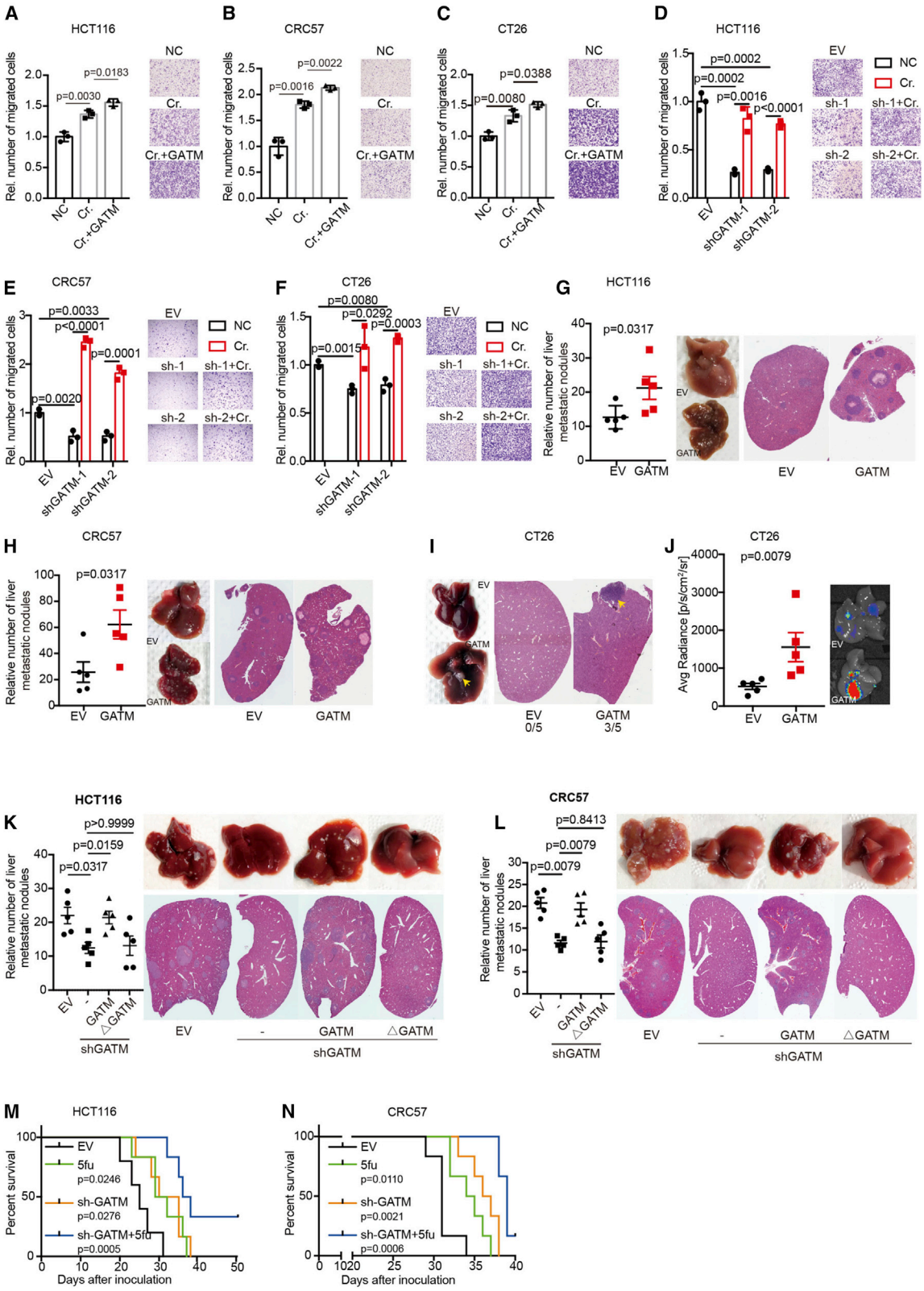

Figure 3. GATM promotes CRC liver metastasis

(A–C) Trans-well migration assay showing migration rates of HCT116, CRC57, and CT26 cells with control (EV) vector or ectopic GATM expression vector (GATM) cultured in regular (NC) or 1 mM creatine-containing (Cr.) medium. Data represent the mean ± SD. p value was calculated based on two-tailed Student's t test.

(legend continued on next page)

Please cite this article in press as: Zhang et al., Creatine promotes cancer metastasis through activation of Smad2/3, Cell Metabolism (2021), https://doi.org/10.1016/j.cmet.2021.03.009

reanalyzed the 273 stage I/II patients from TCGA. Survival probability analysis showed that high levels of GATM were significantly associated with poorer prognosis (Figure 2L).

To investigate whether GATM regulates CRC metastasis, we ectopically expressed GATM in CRC cell lines HCT116, CRC57, and CT26. In addition, we knocked down GATM in these CRC cell lines using two independent shRNAs. The expression and knockdown efficiency were confirmed by western blot (Figures S2D and S2E). The trans-well migration assay showed that creatine treatment and ectopic expression of GATM promoted CRC cell migration (Figures 3A–3C), consistent with the observation that GATM OE enhanced GAA and creatine synthesis (Figures S2F and S2G). Inversely, GATM knockdown (GATM KD) significantly suppressed intracellular creatine levels (Figure S2H) and CRC cell migration, which were rescued by creatine uptake from the cell culture medium (Figures 3D–3F).

We then examined the CRC orthotopic mouse model to assess the influence of GATM on metastasis. GATM OE in all three tested cell lines (HCT116, CRC57, and CT26) enhanced CRC liver metastasis (Figures 3G–3J), whereas GATM KD significantly suppressed CRC liver metastasis with far fewer and much smaller liver metastases than those grown from control cells (Figures S3A–S3C). In contrast, GATM KD did not significantly affect primary tumor growth (Figures S3D and S3E).

To investigate whether GATM-mediated metastasis is enzymatic activity dependent, we mutated the enzymatic site of GATM and introduced the wild-type and mutant GATM into GATM KD HCT116 and CRC57 cells (DesRoches et al., 2016; Stockler-Ipsiroglu et al., 2015). The cells were subsequently injected into mice orthotopically. We observed that knockdown of GATM suppressed cancer metastasis, which was rescued by restoring wild-type GATM, but not the catalytic death GATM (Figures 3K and 3L).

5-Fluorouracil is the frontline chemotherapy drug for advanced and metastatic CRC (Ducreux et al., 2011). We then examined the therapeutic effect of combined GATM KD and 5-fluorouracil treatment in the mice orthotopically implanted with HCT116 and CRC57 cells. We observed that GATM KD alone prolonged mouse survival. Notably, combination GATM KD and 5-fluorouracil further significantly elevated a survival benefit to the mice (Figures 3M and 3N). Taken together, the data show that targeting GATM is potentially complementary to current chemotherapies for CRC treatment.

Creatine and GATM activate Smad2/3 signaling

To investigate whether creatine manipulates signaling pathways that promote tumor metastasis, we performed a phosphorylation multi-pathway profiling array that allows screening 55 phosphorylated human proteins involved in the MAPK, AKT, JAK/STAT, NF-κB, and TGF-β signaling pathways. Among these protein candidates, creatine significantly activated Smad2, a key mediator in TGF-β signaling pathway (Wrighton et al., 2009) (Figures 4A and 4B). To further validate the observation, we treated HCT116 and CT26 cells with creatine and measured phosphorylation of the key Smad proteins in the TGF-β signaling pathway. Western blot showed that creatine not only activated Smad2, but also Smad3 (Figure 4C). Consistently, ectopic expression of GATM also increased the phosphorylation levels of Smad2 and Smad3. The activation of Smad2/3 was further enhanced when the cells were treated with additional creatine (Figure 4D). We then performed quantitative real-time PCR to screen Smad2/3-regulated metastatic genes including Snail, Slug, Vim, Zeb1, Twist1, Tcf3, Six1, Zeb2, and Foxc2 to identify the genes responding to creatine treatment. We found that Snail and Slug were the top creatine-upregulated genes among those tested (Figure 4E). Snail and Slug are well-studied Smad2/3 target genes and have been reported to promote tumor metastasis, including CRC and breast cancer (Cai et al., 2019; Li et al., 2019; Wang et al., 2019; Yeh et al., 2018). To further confirm the upregulation of Snail and Slug mediated by creatine, we treated HCT116 and CT26 cells with creatine. Western blot further confirmed that creatine indeed strongly upregulated the expression of Snail and Slug (Figure 4F). Furthermore, immunohistochemistry staining showed that the expression of Snail and Slug increased in the cecum tumors from the mice fed with creatine compared with regular diet controls (Figure 4G). Taken together, the data show that creatine upregulates Snail and Slug through activation of Smad2 and Smad3.

Creatine activates Smad2/3 signaling via MPS1

Canonically, TGF-β receptor 2 (TGFBR2) phosphorylates TGF-β receptor 1 (TGFBR1) in response to TGF-β. TGFBR1 subsequently phosphorylates Smad2 and Smad3, which is the key step to initiate the TGF-β pathway (Wrighton et al., 2009). Notably, creatine not only increased the phosphorylation of Smad2 and Smad3 in CT26 cells in which both TGFBR1 and TGFBR2 are intact (Holmgaard et al., 2018) but also activated Smad2 and Smad3 in HCT116 cells that harbor a mutant TGFBR2 (de Miranda et al., 2015; Kim et al., 2017; Yi et al., 2017) (Figure 4C). Hence, creatine-induced Smad2/3 phosphorylation must occur through other factors than the TGF-β receptor. Indeed, the TGFBR1 inhibitor SB431542 did not affect creatine-induced Smad2/3 phosphorylation (Figure S4A). Monopolar spindle 1 (MPS1), a protein kinase associated with mitotic progression and spindle checkpoint signaling, has been reported to phosphorylate Smad2 and Smad3 independent of

(D–F) Trans-well migration assay showing migration rates of HCT116, CRC57, and CT26 cells with control (EV) vector or GATM knockdown (sh-1 and sh-2) and cultured in regular or 1 mM creatine-containing medium. Data represent the mean ± SD. p value was calculated based on two-tailed Student's t test.

(G–J) Representative bright-field images, H&E, IVIS luciferase images, and quantification of CRC liver metastasis in mice orthotopically injected with HCT116 (G), CRC57 (H), and CT26 (I and J) cells with control (EV) or ectopic GATM expression (GATM). Error bars denote mean ± SEM of five mice per group. p value was calculated based on Mann-Whitney test.

(K and L) Representative bright-field images, H&E, and quantification of CRC liver metastasis in mice orthotopically injected with HCT116 (K) and CRC57 (L) cells with control (EV) vector or GATM knockdown rescued with wild-type and enzymatical site mutant GATM. Error bars denote mean ± SEM of five mice per group. p value was calculated based on Mann-Whitney test.

(M and N) Survival curve analysis of mice orthotopically injected with control or GATM-knockdown CRC cells HCT116 (M) and CRC57 (N) treated with normal saline or 5-fluorouracil (5FU). p value was calculated based on log-rank test.

Please cite this article in press as: Zhang et al., Creatine promotes cancer metastasis through activation of Smad2/3, Cell Metabolism (2021), https://doi.org/10.1016/j.cmet.2021.03.009

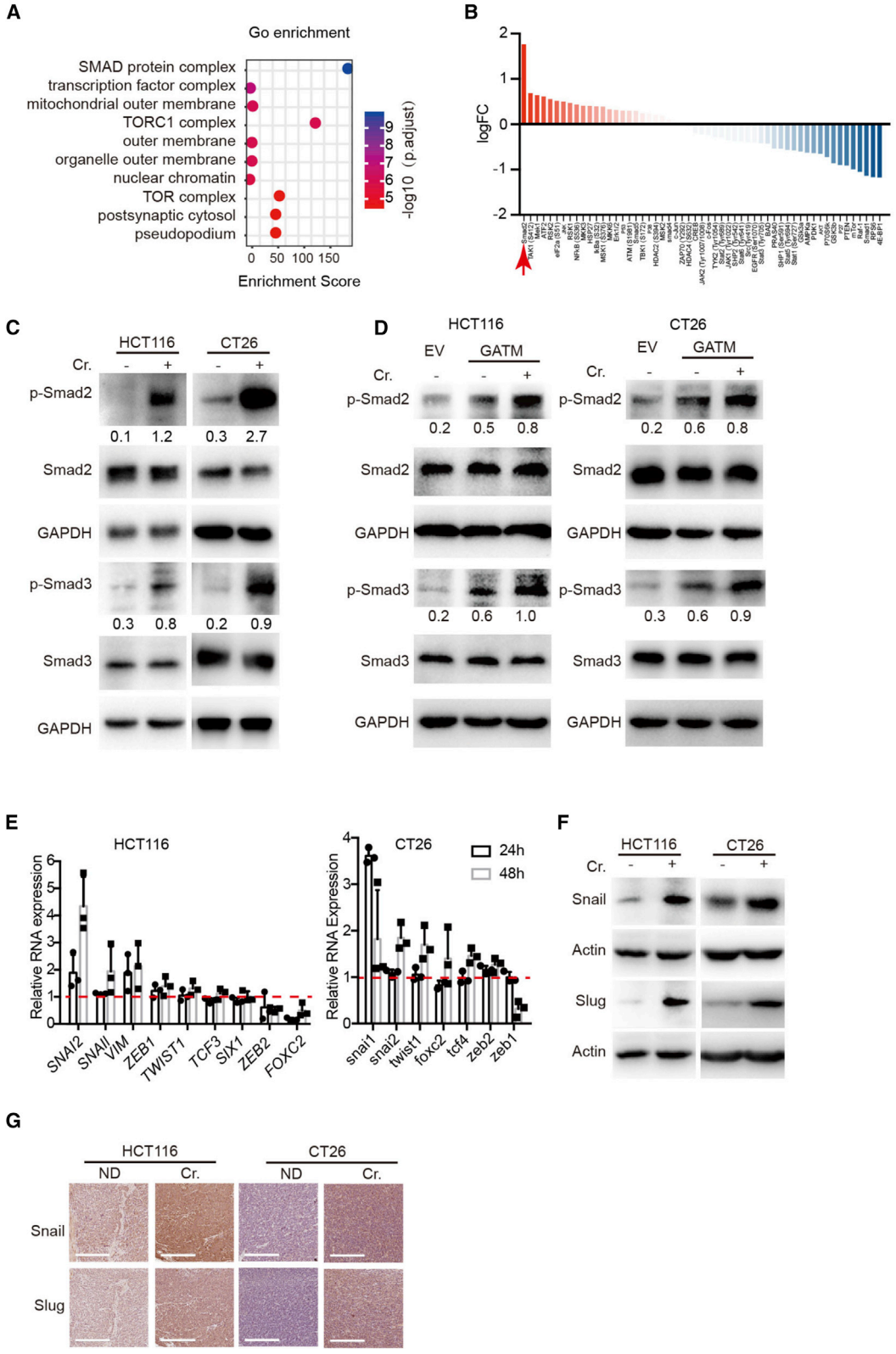

Figure 4. Creatine activates Smad2/3 signaling

(A and B) Gene Ontology enrichment (A) and relative protein phosphorylation level (B) analysis of creatine-activated proteins using a protein phosphorylation array. p value was calculated based on Fisher's exact test.

(legend continued on next page)

Please cite this article in press as: Zhang et al., Creatine promotes cancer metastasis through activation of Smad2/3, Cell Metabolism (2021), https://doi.org/10.1016/j.cmet.2021.03.009

the TGF-β receptor (Hoover and Kubalak, 2008; Zhu et al., 2007). To examine whether creatine facilitates MPS1-mediated Smad2/3 phosphorylation, we applied the MPS1 inhibitor, MPS1-IN-3, to CRC cell lines HCT116 and CT26 and breast cancer cell line 4T1 (Tannous et al., 2013). Western blot showed that MPS1-IN-3 efficiently abrogated creatine-induced Smad2/3 phosphorylation (Figures 5A and S4B). We further knocked down MPS1 in HCT116, CT26, and 4T1 cells (Figure S4C) and treated the cells with creatine, finding that creatine failed to enhance Smad2/3 phosphorylation when MPS1 was knocked down (Figures 5B and S4D). It has been reported that T686 is the key site for human MPS1 activation (Tyler et al., 2009; Wang et al., 2009). Therefore, we mutated the site and introduced the wild-type and mutant MPS1 into MPS1-KD HCT116 cells. We found that creatine significantly elevated Smad2/3 phosphorylation in the cells rescued with wild-type MPS1. In contrast, creatine failed to activate Smad2/3 in the cells rescued with mutant MPS1 (Figure 5C). The essential phosphorylation sites of mouse MPS1 have not been reported. By analyzing the MPS1 protein sequence, we found the identity of mouse MPS1 and human MPS1 reaches 72%. In addition, mouse MPS1 has T675 and T685 sites, in contrast to T676 and T686 in human MPS1 (Figure S4E). We assumed that the T685 site in mouse MPS1 was likely corresponding to T686 in human MPS1. We mutated T685 in mouse MPS1 and introduced the mutant MPS1 into MPS1-KD mouse CRC cells CT26. We observed that creatine elevated Smad2/3 phosphorylation in CT26 cells rescued with wild-type MPS1, but not in the cells rescued with mutant MPS1 (Figure 5D). Together, the data show that creatine activates Smad2/3 via MPS1 and T686 in human MPS1 and T685 in mouse MPS1 are required for creatine-induced Smad2/3 activation.

MPS1 inhibitor suppresses liver metastasis and prolongs mouse survival

To investigate whether inhibition of MPS1 suppresses creatine-enhanced tumor metastasis and benefits survival, we injected MPS1-KD HCT116, CT26, and 4T1 cells into mice orthotopically and fed the mice with creatine-containing diet. We found that MPS1 knockdown significantly suppressed creatine-enhanced cancer metastasis (Figures 5E–5H, S4F, and S4G). In addition, MPS1 knockdown suppressed Snail and Slug expression (Figures 5I, 5J, and S4H) and tumor cell invasion (Figures 5K, 5L, and S4I) in primary tumors. We then investigate the therapeutic potential of MPM1 inhibition. We injected HCT116, CT26, and 4T1 cells into the mice orthotopically and applied 2 mg/kg MPS1-IN-3 by intravenous injection twice per week. We observed that MPS1-IN-3 suppressed cancer invasion and metastasis (Figures S5A–S5D) and Snail/Slug expression in the primary tumors (Figure S5E). In addition, MPS1-IN-3 treatment significantly prolonged the mouse survival time (Figures S5F–S5H). Thus, inhibition of MPS1 suppresses creatine-enhanced invasion and metastasis and prolongs tumor-bearing mouse survival.

DISCUSSION

Creatine is one of the most popular nutrient supplements, widely used to improve muscle mass and function of healthy people (Persky and Brazeau, 2001). In addition, creatine supplementation has also shown promise as an adjunct to medication for the treatment of brain-related disorders such as Huntington's disease and Parkinson's disease (Allen, 2012). In this study, we showed that uptake of creatine significantly enhanced colorectal and breast cancer metastasis and shortened the survival time of the tumor-bearing mice. Notably, the levels of creatine transporter SLC6A8 stay constant in primary tumors and metastases, suggesting that SLC6A8 is likely not the limiting factor in creatine uptake. Therefore, dietary creatine supplements do not benefit every individual. Inversely, long-term uptake of creatine will deteriorate the health status of the cancer patients. In addition to uptake from natural supplements, GATM-mediated *de novo* synthesis of creatine in the tumor cells also significantly promoted tumor metastasis. Inhibition of GATM alone or in combination with 5-fluorouracil significantly suppressed metastasis and prolonged the tumor-bearing mice survival. Thus, GATM may be a potential therapeutic target for cancer metastasis.

In addition to these disease states, previous studies assessed the influence of creatine on tumor growth using subcutaneous injection mouse models which showed that creatine treatment suppressed tumor growth (Di Biase et al., 2019; Kristensen et al., 1999; Miller et al., 1993). Although there is a difference in the efficiency of creatine-mediated tumor growth inhibition between subcutaneous injection and orthotopic mouse models, possibly owing to the different tumor microenvironments, our study also showed that creatine treatment did not benefit primary tumor growth. Especially in CT26- or 4T1-harbored BALB/c mice, creatine suppressed tumor growth in cecum and mammary fad pads, respectively. However, by taking advantage of the orthotopic mouse model, we showed that uptake or *de novo* synthesis of creatine drives tumor invasion and metastasis through the Smad/Snail and Slug axis. Consistent with our observation, accumulating evidences showed that certain treatments did not affect tumor growth in subcutaneous injection mouse models, whereas those same treatments enhanced tumor metastasis in orthotopic mouse models (Nasulewicz et al., 2004; Plantureux et al., 2020; Voloshin et al., 2015). However, other studies showed that alteration of gene expression suppressed primary tumor growth, while promoting tumor metastasis (Massague, 2008; Sun et al., 2018).

It is well known that elevated TGF-β signaling promotes CRC metastasis (Jung et al., 2017). Canonical TGF-β signaling

(C) Western blot showing phosphorylation levels of Smad2 and Smad3 in HCT116 and CT26 cells treated with creatine (1 mM).
(D) Western blot showing phosphorylation levels of Smad2 and Smad3 in HCT116 and CT26 cells with ectopic GATM expression in the presence or absence of creatine (1 mM) treatment.
(E) Quantitative real-time PCR showing the expression levels of Smad2/3 target genes in HCT116 cells and CT26 cells treated with creatine.
(F) Western blot showing expression levels of Snail and Slug expression in HCT116 and CT26 treated with creatine (1 mM).
(G) Immunohistochemistry measuring Snail and Slug expression in primary CRCs from mice orthotopically injected with HCT116 and CT26 cells and fed with normal diet (ND) or creatine-supplemented diet (Cr.). Scale bar, 300 μm.

Please cite this article in press as: Zhang et al., Creatine promotes cancer metastasis through activation of Smad2/3, Cell Metabolism (2021), https://doi.org/10.1016/j.cmet.2021.03.009

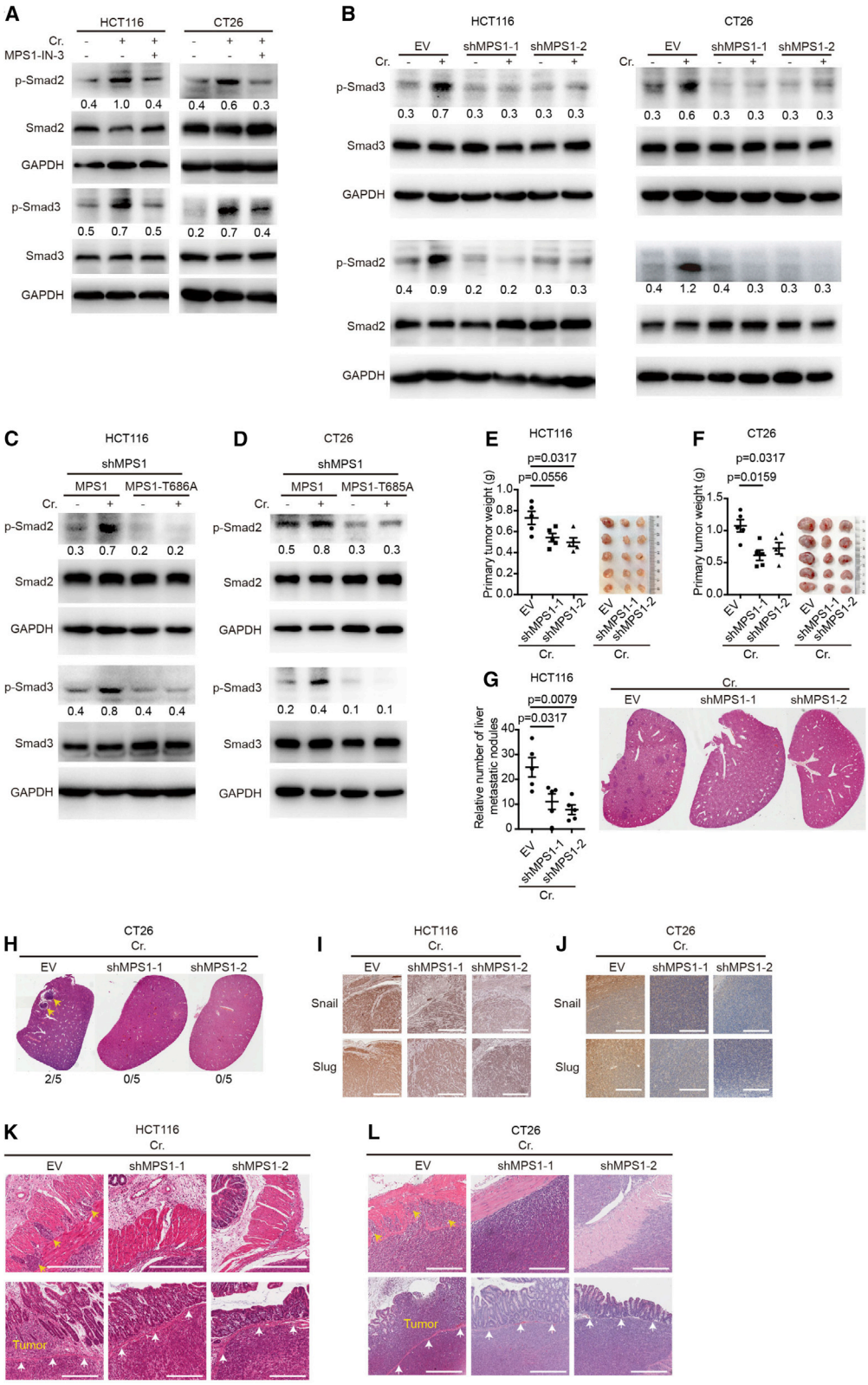

(legend on next page)

Please cite this article in press as: Zhang et al., Creatine promotes cancer metastasis through activation of Smad2/3, Cell Metabolism (2021), https://doi.org/10.1016/j.cmet.2021.03.009

requires the activation of Smad2 and Smad3, which are phosphorylated by TGFBR1 and TGFBR2 (Wrighton et al., 2009). However, TGF-β signaling is still active in some of the CRCs that harbor mutant TGF-β receptors (de Miranda et al., 2015). Studies showed that MPS1 activated the TGF-β pathway through the phosphorylation of Smad2 and Smad3 independent of TGF-β receptors (Zhu et al., 2007). However, it remains to be elucidated as to what triggers MPS1 to phosphorylate Smad2 and Smad3. In this study, we showed that creatine significantly enhanced Smad2 and Smad3 phosphorylation through MPS1. Moreover, inhibition of MPS1 strongly suppressed Snail and Slug expression and prolonged mouse survival. Of note, more than 80% of CRC with microsatellite instability harbors mutations in TGFBR2, and mutations in TGFBR1 are also frequently detected in CRC (de Miranda et al., 2015). Therefore, inhibition of MPS1 may be an effective strategy to suppress cancer metastasis, especially for the CRCs with TGF-β receptor mutation.

Limitations of study

Our study shows the risk of taking creatine supplementation for the cancer patients to suppress tumor growth or reverse cachexia. Additional creatine supplement likely does not benefit recovery of the patients and instead will promote cancer metastasis. However, given that creatine supplement is important for increasing muscle strength and improving brain function, restriction of creatine supplement may not be a good strategy for cancer patients to suppress metastasis. Similarly, targeting GATM likely causes side effects, especially for the vegan patients who gain creatine mainly through intrinsic synthesis. Thus, targeting MPS1 is an alternative approach against cancer metastasis.

Cellular heterogeneity generally exists in many types of cancers including CRC and presents a leading challenge for effective therapy. The heterogeneous cells transition between different states, pose heterogenic biosynthetic capacities (McGranahan and Swanton, 2017), and likely have different efficiency of creatine uptake or synthesis. It will be interesting to investigate whether creatine transforms or elevates certain cell populations in CRC, leading to more metastasis. Consistent with this possibility, creatine has been reported to improve neural progenitor cell survival in Huntington's disease (Andres et al., 2016). We showed that creatine upregulated Snail/Slug expression, a feature of epithelial-mesenchymal transition.

Increasing evidence shows that metabolites are important to regulate cancer development. Further studies show that many metabolites are involved in manipulating cell signaling, such as mTOR, MAPK, and NF-kB (Deldicque et al., 2007; Elia et al., 2018; Pazini et al., 2016). However, owing to technological barriers, the mechanism of modification and regulation of specific genes has only been identified for a number of metabolites. Here, we showed that creatine-induced smad2/3 phosphorylation dependent on T686 in human MPS1 and T685 in mouse MPS1. However, it is still unclear precisely how creatine regulates MPS1 activity, which we strongly intend to understand in the following study.

STAR★METHODS

Detailed methods are provided in the online version of this paper and include the following:

- KEY RESOURCES TABLE
- RESOURCE AVAILABILITY
  - Lead Contact
  - Materials Availability
  - Data and Code Availability
- EXPERIMENTAL MODEL AND SUBJECT DETAILS
  - Cell culture, lentiviral vector and infection
  - Animal and diets
  - Patients specimens
- METHOD DETAILS
  - RT-qPCR
  - GAA and Creatine measurement by CE-MS
  - Trans-well migration assay
  - Western blot
  - Immunohistochemistry
  - Cecum injection and mammary fat pad injection
  - Human phosphorylation multi-pathway profiling array
- QUANTIFICATION AND STATISTICAL ANALYSIS
  - Quantification of metastasis
  - Analysis of tissue microarray
  - Meta-analysis

Figure 5. Creatine promotes cancer metastasis through MPS1-activated Smas2/3 signaling

(A) Western blot showing phosphorylation levels of Smad2 and Smad3 in HCT116 and CT26 cells treated with MPS1 inhibitor (MPS1-IN-3).

(B) Western blot showing phosphorylation levels of Smad2 and Smad3 in HCT116 and CT26 cells with control (EV) vector or MPS1 knockdown (shMPS1-1 and shMPS1-2) in the presence or absence of creatine (1 mM) treatment.

(C and D) Western blot showing phosphorylation levels of Smad2 and Smad3 in HCT116 and CT26 cells with MPS1 knockdown rescued by wild-type MPS1 or mutant MPS1 in the presence or absence of creatine (1 mM) treatment.

(E and F) Representative bright-field images and quantification of tumor weight of primary CRC growth in NSG mice orthotopically injected with HCT116 (E) and CRC57 cells (F) with control (EV) vector or MPS1 knockdown (shMPS1-1 and shMPS1-2) when the mice were treated with creatine. Error bars denote mean ± SEM of five mice per group. p value was calculated based on Mann-Whitney test.

(G and H) Representative H&E and quantification of CRC liver metastasis in mice orthotopically injected with HCT116 (G) and CT26 (H) cells with control (EV) vector or MPS1 knockdown (shMPS1-1 and shMPS1-2) when the mice were treated with creatine. Error bars denote mean ± SEM of five mice per group. p value was calculated based on Mann-Whitney test.

(I and J) Representative immunohistochemistry images for measuring expression levels of Snail and Slug in primary CRC tumor in NSG mice orthotopically injected with HCT116 (I) and CT26 (J) cells with control (EV) vector or MPS1 knockdown (shMPS1-1 and shMPS1-2) when the mice were treated with creatine. Scale bar, 300 μm.

(K and L) Representative H&E images showing primary tumor invasion in the mice with cecum injection of HCT116 (K) and CT26 (L) cells with control (EV) vector or MPS1 knockdown (shMPS1-1 and shMPS1-2) when the mice were treated with creatine. Yellow arrows indicate invasive tumor, and white arrows indicate muscularis mucosae. Scale bars, upper, 400 μm; lower, 200 μm.

- Statistical Analyses

SUPPLEMENTAL INFORMATION

Supplemental information can be found online at https://doi.org/10.1016/j.cmet.2021.03.009.

ACKNOWLEDGMENTS

We thank Professors Zusen Fan (Institute of Biophysics, Chinese Academy of Sciences) and Xiling Shen (Duke University) for reading our manuscript and providing suggestions. This project was partly supported by the Strategic Priority Research Program of the Chinese Academy of Sciences (XDB29040100), the Chinese Ministry of Science and Technology (2017YFA0504103), and the National Natural Science Foundation of China (31771513, 81972797, 81921003, 81870393, 81571563, and 82000812).

AUTHOR CONTRIBUTIONS

L.Z. and P.B. came up with the concept, designed the experiments, and wrote the manuscript. L.Z. performed most experiments with assistance from H.Y. and Z.W. for animal experiments, Z.Z. and X.Z. for western blot, Q.Z. and P.G. for some molecular cloning, and F.Z. for data analysis. J.D. and H.C. provided the patient samples. W.W. and H.-L.P. performed CE-MS analysis. D.H. created the CRC PDX cell line. G.S. analyzed the tissue microarray data.

DECLARATION OF INTERESTS

The authors declare no competing interests.

Received: August 25, 2020
Revised: February 15, 2021
Accepted: March 11, 2021
Published: April 2, 2021

REFERENCES

Allen, P.J. (2012). Creatine metabolism and psychiatric disorders: does creatine supplementation have therapeutic value? Neurosci Biobehav Rev *36*, 1442–1462.

Andres, R.H., Wallimann, T., and Widmer, H.R. (2016). Creatine supplementation improves neural progenitor cell survival in Huntington's disease. Brain Circ *2*, 133–137.

Bu, P., Wang, L., Chen, K.Y., Rakhilin, N., Sun, J., Closa, A., Tung, K.L., King, S., Kristine Varanko, A., Xu, Y., et al. (2015). miR-1269 promotes metastasis and forms a positive feedback loop with TGF-β. Nat. Commun. *6*, 6879.

Bu, P., Chen, K.Y., Xiang, K., Johnson, C., Crown, S.B., Rakhilin, N., Ai, Y., Wang, L., Xi, R., Astapova, I., et al. (2018). Aldolase B-mediated fructose metabolism drives metabolic reprogramming of colon cancer liver metastasis. Cell Metab *27*, 1249–1262.e4.

Cai, J., Xia, L., Li, J., Ni, S., Song, H., and Wu, X. (2019). Tumor-associated macrophages derived TGF-β–I induced epithelial to mesenchymal transition in colorectal cancer cells through Smad2,3–4/snail signaling pathway. Cancer Res. Treat. *51*, 252–266.

Chen, R., Wang, J., Zhan, R., Zhang, L., and Wang, X. (2019). Integrated systems pharmacology, urinary metabonomics, and quantitative real-time PCR analysis to uncover targets and metabolic pathways of the You-Gui pill in treating kidney-Yang deficiency syndrome. Int. J. Mol. Sci. *20*.

de Miranda, N.F., van Dinther, M., van den Akker, B.E., van Wezel, T., ten Dijke, P., and Morreau, H. (2015). Transforming growth factor beta signaling in colorectal cancer cells with microsatellite instability despite biallelic mutations in TGFBR2. Gastroenterology *148*, 1427–1437.e8.

Deldicque, L., Theisen, D., Bertrand, L., Hespel, P., Hue, L., and Francaux, M. (2007). Creatine enhances differentiation of myogenic C2C12 cells by activating both p38 and Akt/PKB pathways. Am. J. Physiol. Cell Physiol. *293*, C1263–C1271.

DesRoches, C.L., Bruun, T., Wang, P., Marshall, C.R., and Mercimek-Mahmutoglu, S. (2016). Arginine-glycine amidinotransferase deficiency and functional characterization of missense variants in GATM. Hum. Mutat. *37*, 926–932.

Di Biase, S., Ma, X., Wang, X., Yu, J., Wang, Y.C., Smith, D.J., Zhou, Y., Li, Z., Kim, Y.J., Clarke, N., et al. (2019). Creatine uptake regulates CD8 T cell antitumor immunity. J. Exp. Med. *216*, 2869–2882.

Ducreux, M., Bennouna, J., Hebbar, M., Ychou, M., Lledo, G., Conroy, T., Adenis, A., Faroux, R., Rebischung, C., Bergougnoux, L., et al. (2011). Capecitabine plus oxaliplatin (XELOX) versus 5-fluorouracil/leucovorin plus oxaliplatin (FOLFOX-6) as first-line treatment for metastatic colorectal cancer. Int. J. Cancer *128*, 682–690.

Dueland, S., Guren, T.K., Hagness, M., Glimelius, B., Line, P.D., Pfeiffer, P., Foss, A., and Tveit, K.M. (2015). Chemotherapy or liver transplantation for nonresectable liver metastases from colorectal cancer? Ann. Surg. *261*, 956–960.

Elia, I., Doglioni, G., and Fendt, S.M. (2018). Metabolic hallmarks of metastasis formation. Trends Cell Biol *28*, 673–684.

Fu, X.Y., Besterman, J.M., Monosov, A., and Hoffman, R.M. (1991). Models of human metastatic colon cancer in nude mice orthotopically constructed by using histologically intact patient specimens. Proc. Natl. Acad. Sci. USA *88*, 9345–9349.

Guan, X. (2015). Cancer metastases: challenges and opportunities. Acta Pharmacol. Sin. B *5*, 402–418.

Holmgaard, R.B., Schaer, D.A., Li, Y., Castaneda, S.P., Murphy, M.Y., Xu, X., Inigo, I., Dobkin, J., Manro, J.R., Iversen, P.W., et al. (2018). Targeting the TGFβ pathway with galunisertib, a TGFβRI small molecule inhibitor, promotes anti-tumor immunity leading to durable, complete responses, as monotherapy and in combination with checkpoint blockade. J. Immunother. Cancer *6*, 47.

Hoover, L.L., and Kubalak, S.W. (2008). Holding their own: the noncanonical roles of Smad proteins. Sci. Signal. *1*, pe48.

Ireson, C.R., Alavijeh, M.S., Palmer, A.M., Fowler, E.R., and Jones, H.J. (2019). The role of mouse tumour models in the discovery and development of anticancer drugs. Br. J. Cancer *121*, 101–108.

Jiang, H., Wang, P., Wang, Q., Wang, B., Mu, J., Zhuang, X., Zhang, L., Yan, J., Miller, D., and Zhang, H.G. (2014). Quantitatively controlling expression of miR-17~92 determines colon tumor progression in a mouse tumor model. Am. J. Pathol. *184*, 1355–1368.

Jung, B., Staudacher, J.J., and Beauchamp, D. (2017). Transforming growth factor β superfamily signaling in development of colorectal cancer. Gastroenterology *152*, 36–52.

Kim, K.H., Han, J.W., Jung, S.K., Park, B.J., Han, C.W., and Joo, M. (2017). Kaurenoic acid activates TGF-beta signaling. Phytomedicine *32*, 8–14.

Kristensen, C.A., Askenasy, N., Jain, R.K., and Koretsky, A.P. (1999). Creatine and cyclocreatine treatment of human colon adenocarcinoma xenografts: 31P and 1H magnetic resonance spectroscopic studies. Br. J. Cancer *79*, 278–285.

Kulaylat, M.N., and Gibbs, J.F. (2010). Regional treatment of colorectal liver metastasis. J. Surg. Oncol. *101*, 693–698.

Li, H., Zhang, Z., Chen, L., Sun, X., Zhao, Y., Guo, Q., Zhu, S., Li, P., Min, L., and Zhang, S. (2019). Cytoplasmic asporin promotes cell migration by regulating TGF-β/Smad2/3 pathway and indicates a poor prognosis in colorectal cancer. Cell Death Dis *10*, 109.

Massague, J. (2008). TGFbeta in cancer. Cell *134*, 215–230.

McGranahan, N., and Swanton, C. (2017). Clonal heterogeneity and tumor evolution: past, present, and the future. Cell *168*, 613–628.

Miller, E.E., Evans, A.E., and Cohn, M. (1993). Inhibition of rate of tumor growth by creatine and cyclocreatine. Proc. Natl. Acad. Sci. USA *90*, 3304–3308.

Nasulewicz, A., Wietrzyk, J., Wolf, F.I., Dzimira, S., Madej, J., Maier, J.A., Rayssiguier, Y., Mazur, A., and Opolski, A. (2004). Magnesium deficiency inhibits primary tumor growth but favors metastasis in mice. Biochim. Biophys. Acta *1739*, 26–32.

Norman, K., Stübler, D., Baier, P., Schütz, T., Ocran, K., Holm, E., Lochs, H., and Pirlich, M. (2006). Effects of creatine supplementation on nutritional status,

muscle function and quality of life in patients with colorectal cancer–a double blind randomised controlled trial. Clin. Nutr. *25*, 596–605.

Pazini, F.L., Cunha, M.P., Rosa, J.M., Colla, A.R.S., Lieberknecht, V., Oliveira, Á., and Rodrigues, A.L.S. (2016). Creatine, similar to ketamine, counteracts depressive-like behavior induced by corticosterone via PI3K/Akt/mTOR pathway. Mol. Neurobiol. *53*, 6818–6834.

Persky, A.M., and Brazeau, G.A. (2001). Clinical pharmacology of the dietary supplement creatine monohydrate. Pharmacol. Rev. *53*, 161–176.

Plantureux, L., Mège, D., Crescence, L., Carminita, E., Robert, S., Cointe, S., Brouilly, N., Ezzedine, W., Dignat-George, F., Dubois, C., and Panicot-Dubois, L. (2020). The interaction of platelets with colorectal cancer cells inhibits tumor growth but promotes metastasis. Cancer Res *80*, 291–303.

Rawla, P., Sunkara, T., and Barsouk, A. (2019). Epidemiology of colorectal cancer: incidence, mortality, survival, and risk factors. Prz. Gastroenterol. *14*, 89–103.

Secker, P.F., Luks, L., Schlichenmaier, N., and Dietrich, D.R. (2018). RPTEC/TERT1 cells form highly differentiated tubules when cultured in a 3D matrix. ALTEX *35*, 223–234.

Stockler-Ipsiroglu, S., Apatean, D., Battini, R., DeBrosse, S., Dessoffy, K., Edvardson, S., Eichler, F., Johnston, K., Koeller, D.M., Nouioua, S., et al. (2015). Arginine:glycine amidinotransferase (AGAT) deficiency: clinical features and long term outcomes in 16 patients diagnosed worldwide. Mol. Genet. Metab. *116*, 252–259.

Sun, X., Wang, S.C., Wei, Y., Luo, X., Jia, Y., Li, L., Gopal, P., Zhu, M., Nassour, I., Chuang, J.-C., et al. (2018). Arid1a has context-dependent oncogenic and tumor suppressor functions in liver cancer. Cancer Cell *33*, 151–152.

Tannous, B.A., Kerami, M., Van der Stoop, P.M., Kwiatkowski, N., Wang, J., Zhou, W., Kessler, A.F., Lewandrowski, G., Hiddingh, L., Sol, N., et al. (2013). Effects of the selective MPS1 inhibitor MPS1-IN-3 on glioblastoma sensitivity to antimitotic drugs. J. Natl. Cancer Inst. *105*, 1322–1331.

Tyler, R.K., Chu, M.L., Johnson, H., McKenzie, E.A., Gaskell, S.J., and Eyers, P.A. (2009). Phosphoregulation of human Mps1 kinase. Biochem. J. *417*, 173–181.

Valsecchi, F., Konrad, C., D'Aurelio, M., Ramos-Espiritu, L.S., Stepanova, A., Burstein, S.R., Galkin, A., Magranè, J., Starkov, A., Buck, J., et al. (2017). Distinct intracellular sAC-cAMP domains regulate ER Ca2+ signaling and OXPHOS function. J. Cell Sci. *130*, 3713–3727.

Voloshin, T., Alishekevitz, D., Kaneti, L., Miller, V., Isakov, E., Kaplanov, I., Voronov, E., Fremder, E., Benhar, M., Machluf, M., et al. (2015). Blocking IL1beta pathway following paclitaxel chemotherapy slightly inhibits primary tumor growth but promotes spontaneous metastasis. Mol. Cancer Ther. *14*, 1385–1394.

Wang, W., Yang, Y.T., Gao, Y.F., Xu, Q.B., Wang, F., Zhu, S.C., Old, W., Resing, K., Ahn, N., Lei, M., and Liu, X. (2009). Structural and mechanistic insights into Mps1 kinase activation. J. Cell. Mol. Med. *13*, 1679–1694.

Wang, X., Liu, R., Zhu, W., Chu, H., Yu, H., Wei, P., Wu, X., Zhu, H., Gao, H., Liang, J., et al. (2019). UDP-glucose accelerates SNAI1 mRNA decay and impairs lung cancer metastasis. Nature *571*, 127–131.

Wang, C.H., Lundh, M., Fu, A., Kriszt, R., Huang, T.L., Lynes, M.D., Leiria, L.O., Shamsi, F., Darcy, J., Greenwood, B.P., et al. (2020a). CRISPR-engineered human brown-like adipocytes prevent diet-induced obesity and ameliorate metabolic syndrome in mice. Sci. Transl. Med. *12*.

Wrighton, K.H., Lin, X., and Feng, X.H. (2009). Phospho-control of TGF-beta superfamily signaling. Cell Res *19*, 8–20.

Wyss, M., and Kaddurah-Daouk, R. (2000). Creatine and creatinine metabolism. Physiol. Rev. *80*, 1107–1213.

Yan, M., Qi, H., Xia, T., Zhao, X., Wang, W., Wang, Z., Lu, C., Ning, Z., Chen, H., Li, T., et al. (2019). Metabolomics profiling of metformin-mediated metabolic reprogramming bypassing AMPKα. Metabolism *91*, 18–29.

Yeh, H.-W., Hsu, E.-C., Lee, S.-S., Lang, Y.-D., Lin, Y.-C., Chang, C.-Y., Lee, S.-Y., Gu, D.-L., Shih, J.-H., Ho, C.-M., et al. (2018). PSPC1 mediates TGF-beta1 autocrine signalling and Smad2/3 target switching to promote EMT, stemness and metastasis. Nat. Cell Biol. *20*, 479–491.

Yi, H., Geng, L., Black, A., Talmon, G., Berim, L., and Wang, J. (2017). The miR-487b-3p/GRM3/TGFbeta signaling axis is an important regulator of colon cancer tumorigenesis. Oncogene *36*, 3477–3489.

Zacharakis, M., Xynos, I.D., Lazaris, A., Smaro, T., Kosmas, C., Dokou, A., Felekouras, E., Antoniou, E., Polyzos, A., Sarantonis, J., et al. (2010). Predictors of survival in stage IV metastatic colorectal cancer. Anticancer Res *30*, 653–660.

Zeng, J., Yin, P., Tan, Y., Dong, L., Hu, C., Huang, Q., Lu, X., Wang, H., and Xu, G. (2014). Metabolomics study of hepatocellular carcinoma: discovery and validation of serum potential biomarkers by using capillary electrophoresis-mass spectrometry. J. Proteome Res. *13*, 3420–3431.

Zhang, C.-S., Hawley, S.A., Zong, Y., Li, M., Wang, Z., Gray, A., Ma, T., Cui, J., Feng, J.-W., Zhu, M., et al. (2017). Fructose-1,6-bisphosphate and aldolase mediate glucose sensing by AMPK. Nature *548*, 112–116.

Zhu, S., Wang, W., Clarke, D.C., and Liu, X. (2007). Activation of Mps1 promotes transforming growth factor-beta-independent Smad signaling. J. Biol. Chem. *282*, 18327–18338.

Please cite this article in press as: Zhang et al., Creatine promotes cancer metastasis through activation of Smad2/3, Cell Metabolism (2021), https://doi.org/10.1016/j.cmet.2021.03.009

STAR★METHODS

KEY RESOURCES TABLE

REAGENT or RESOURCE	SOURCE	IDENTIFIER
Antibodies		
Rabbit anti-GATM	Sigma	Cat# HPA026077; RRID: AB_1849528
Rabbit anti-Phospho-Smad2	CST	Cat# 3108; RRID: AB_490941
Rabbit anti-Phospho-Smad3	CST	Cat# 9520; RRID: AB_2193207
Rabbit anti-Smad2	Abcam	Cat# ab33875; RRID: AB_777976
Rabbit anti-Smad3	Abcam	Cat# ab40854; RRID: AB_777979
Rabbit anti-Snail	ABclonal	Cat# A12301; RRID: AB_2759158
Rabbit anti-Slug	ABclonal	Cat# A1057; RRID: AB_2758111
Rabbit anti-MPS1	CST	Cat# 5469; RRID: AB_10692670
Rabbit anti-SLC6A8	Abcam	Cat# ab62196; RRID: AB_956305
Rabbit anti-Actin	ABclonal	Cat# AC026; RRID: AB_2768234
Mouse anti-GAPDH	ABclonal	Cat# AC033; RRID: AB_2769570
Goat HRP-goat anti Rabbit IgG	EMAR	Cat# EM35111; RRID: AB_2572420
Goat HRP-goat anti Mouse IgG	EMAR	Cat# EM35110; RRID: AB_2890177
Chemicals, Peptides, and Recombinant Proteins		
RPMI 1640 medium	Thermo	C11875500BT
DMEM	Thermo	C11965500BT
TRIzol	Thermo Fisher Scientific	15596
HiScript II Q RT SuperMix	Vazyme	R223
Cutoff filter	Millipore	UFC3LCCNB-HMT
Lysis buffe	Thermo	89900
Protease inhibitors	Roche	4693132001
HRP-conjugated secondary antibody	Zsbio	6001&6002
DAB	Zsbio	9019
Hematoxylin staining	Zsbio	9610
Creatine monohydrate	Sigma	c3630
5-fluorouracil	Sigma	F6627
MPS1-IN-3	MCE	1609584-72-6
creatine monohydrate	Sigma	C3630
Critical Commercial Assays		
QuikChange Multi Site Directed Mutagenesis kit	Agilent	200514
RNeasy Mini Kit	Qiagen	74104
Pierce BCA Protein Assay Kit	Thermo Scientific	23225
Experimental Models: Cell Lines		
CRC57	Gift form David Hsu	Bu et al., 2018
HCT116	ATCC	Cat#CCL-247
CT26	ATCC	Cat#CRL-2638
4T1	ATCC	Cat#CRL-2539
HEK293T	ATCC	Cat#CRL-3216
Experimental Models: Organisms/Strains		
Mouse: BALB/c	Gem Pharmatech	N000020
Mouse: NSG	Gem Pharmatech	T001475
Oligonucleotides		
shRNA sequences and RT-qPCR primer sequences	Table S3, This study	N/A

(*Continued on next page*)

Please cite this article in press as: Zhang et al., Creatine promotes cancer metastasis through activation of Smad2/3, Cell Metabolism (2021), https://doi.org/10.1016/j.cmet.2021.03.009

Continued

REAGENT or RESOURCE	SOURCE	IDENTIFIER
Recombinant DNA		
pLKO.1	This study	N/A
pCDH	This study	N/A
psPAX2	Addgene	12260
pMD2.G	Addgene	12259
NL4-3 mCherry Luciferase	Addgene	44965
Software and Algorithms		
Image J	NIH	https://imagej.nih.gov/ij/
Prism 7	GraphPad	https://www.graphpad.com/scientific-software/prism/
Other		
5% w/w creatine monohydrate supplement diet	Beijing HFK Bioscience	N/A
Human phosphorylation multi-pathway profiling array C55	RayBiotech	AAH-PPP-1-2

RESOURCE AVAILABILITY

Lead Contact

Further information and requests for resources and reagents should be directed to and will be fulfilled by the Lead Contact, Pengcheng Bu (bupc@ibp.ac.cn).

Materials Availability

All the materials generated in this study are available upon reasonable request to the Lead Contact.

Data and Code Availability

All datasets used in the manuscript are publicly available.

EXPERIMENTAL MODEL AND SUBJECT DETAILS

Cell culture, lentiviral vector and infection

Human CRC cell HCT116, mouse colon cancer cell CT26, and mouse breast cancer cell 4T1 were obtained from American Type Culture Collection (ATCC). Patient derived xenograft CRC cell CRC57 was obtained as described previously (Bu et al., 2018). HCT116 and CRC57 cells were originally derived from male colorectal cancer patients. 4T1 and CT26 cells were originally derived from female BALB/c mice. The cell lines were grown in RPMI 1640 medium with 10% FBS and 1% penicillin-streptomycin. 293T cells for virus production were cultured in DMEM with high glucose supplemented with 10% FBS and 1% penicillin-streptomycin. All cell lines were maintained at 37°C with 5% CO_2 and routinely tested for mycoplasma contamination by PCR. shRNAs against GATM, SLC6A8, and MPS1 were cloned into the lentiviral vector pLKO.1. Mutant GATM (R413W), human MPS1 (hMPS1, T686A), and mouse MPS1 (mMPS1, T685A) were generated by QuikChange Multi Site Directed Mutagenesis kit (200514, Agilent). Wild-type GATM and the mutants were cloned into the lentiviral vector pCDH. The lentiviral constructs were co-transfected with helper plasmids into 293T cells. The virus was collected 48 hours after transfection and used to infect the cells. shRNAs sequences were shown in Table S3.

Animal and diets

Mouse maintenance and procedures were approved by the Biomedical Research Ethics Committee of the Institute of Biophysics, Chinese Academy of Sciences. The experimental procedures were performed by following the relevant ethical regulations regarding animal research. Seven-week-old female NSG and BALB/c mice were used throughout the study. All mice were maintained in a specific-pathogen free facility with a 12h:12h light: dark cycle at 21-23°C. All mice were routinely checked by certified veterinarians and healthy prior to the tumor-bearing experiments. After transplanted tumor cells, the mice were monitored daily for any signs of suffering or abnormal behavior. Randomized groups of mice were treated with creatine supplement one week after tumor cell implantation in two ways. In the first way, the mice were fed with a 5% w/w creatine monohydrate supplement diet or regular diet (1022, Beijing HFK Bioscience). In the second way, the mice were fed with creatine-containing water (42.5 mg/ml, 400 ml/time, 3 times per week) or control water by oral gavage. Creatine monohydrate (c3630, Sigma) was used in this study and validated with $\geq$98% purity. For the mouse treatment, 5-fluorouracil (F6627, Sigma), at a dose of 12.5 mg/kg in saline or vehicle control, were used through the intraperitoneal route twice a week. MPS1-IN-3 (1609584-72-6, MCE), at a dose of 2 mg/kg or vehicle control, were used through the intravenous route twice a week.

Please cite this article in press as: Zhang et al., Creatine promotes cancer metastasis through activation of Smad2/3, Cell Metabolism (2021), https://doi.org/10.1016/j.cmet.2021.03.009

Patients specimens

The primary and liver metastatic CRC specimens were obtained from the 7th medical center of PLA general hospital with informed consent from all donors. All studies were approved by the Ethics Committee of the 7th Medical Center of PLA General Hospital and the Institute of Biophysics, Chinese Academy of Sciences. The patient information is shown in Table S2. Samples from 52% male and 48% female patients with age from 34 to 84 years old (mean age as 62) were included in this study.

METHOD DETAILS

RT-qPCR

RNA was isolated using TRIzol (15596, Thermo Fisher Scientific) or RNeasy Mini Kit (74104, Qiagen) and evaluated by agarose gel electrophoresis and the ratio of 260/280 and 260/230. cDNA was synthesized using HiScript II Q RT SuperMix (R223, Vazyme) and DNA was removed by adding DNase. RT-qPCR was performed on the QuantStudio 3 real-time PCR instrument using the primers shown in Table S3. All paired primers are exon-exon junction primers. The primer sets were widely used in previous publications (Chen et al., 2019; Jiang et al., 2014; Secker et al., 2018; Valsecchi et al., 2017; Wang et al., 2019, 2020) and were further validated by amplifying a series of dilution of template cDNA. The expression of each gene was defined from the threshold cycle (Ct) and the relative levels were caltulated using the 2-ΔΔCt method and normalized to the levels of actin.

GAA and Creatine measurement by CE-MS

GAA and creatine levels were measured by capillary electrophoresis-mass spectrometry (CE-MS) based metabolite analysis on CE (G7100A, Agilent) coupled with time-of-flight (TOF) MS (G6224A, Agilent). The sample preparation for CE-MS was carried out as described previously (Yan et al., 2019; Zhang et al., 2017) with slight modifications. In brief, cell samples collected from a 10-cm dish (70–80% confluence) or 10 mg tumor tissue samples were used for each measurement. After bring the volume to 20 ml of 5% mannitol solution (dissolved in water), the cells were instantly frozen in liquid nitrogen, followed by lysing with 1 ml of methanol containing internal standards 1 (IS1, H3304-1002, Human Metabolome Technologies, 1:200, used to standardize the metabolite intensity and to adjust the migration time), and mixing with 1 ml chloroform by 20 seconds of vortexing. The cell lysates had 400 μl of water subsequently added and further vortexed for 20 seconds. After centrifugation at 15,000 g for 15 minutes at 4 °C, 400 μl of aqueous phase was collected, filtered and freeze-dried. The freshly excised tumor tissues were immediately frozen in liquid nitrogen, and ground in 600 μl of methanol containing 50 μM IS1. The lysates were then mixed with 600 μl chloroform and 240 μl water by 20 seconds of vortexing. After centrifugation, 400 μl of aqueous phase was collected and filtered through a 5-kDa cutoff filter (UFC3LCCNB-HMT, Millipore) by centrifuging at 12,000 g for 3 hours at 4 °C. In addition, 100 μl of the aqueous phase from each sample were combined and filtered, used for quality control (QC). The filtered aqueous phase was then freeze-dried in a vacuum concentrator and then dissolved in water containing IS3 (H3304-1104, Human Metabolome Technologies, 1:200) to adjust the migration time. 10 μl of re-dissolved solution was then loaded into an injection vial with a conical insert for CE–TOF MS analysis. The fused silica capillary (50 μm i.d. × 80 cm, Human Metabolome Technologies, Tsuruoka, Japan) was used for sample separation. CE-MS analysis was carried out as described previously (Zeng et al., 2014). The qualitative analysis proceeded based on the pre-analyzed metabolite standard library (HMT), and identified the GAA and creatine at m/z 118.0611 and m/z 132.0768, respectively. Peak extraction and identification were carried out with Quantitative Analysis Software (Agilent). The quantity of GAA and creatine were normalized by total peak area of whole metabolites from a cell sample and the quantity of creatine were normalized by peak area of internal standard and dry weight of cell or tissue sample.

Trans-well migration assay

4×10^4 HCT116, CRC57, or CT26 cells were plated in the upper chamber (MAMI C8S 10, Millipore) with serum-free medium. The lower chamber was filled with medium containing 10% FBS. Twelve hours later, non-migrated cells on the upper side of the filter were removed with a cotton swab, and cells on the underside of the filter were stained with 0.5% crystal violet and calculated under a microscope. For each experiment, the number of cells in nine random fields were counted, and three independent filters were analyzed.

Western blot

Whole cell lysate was prepared in lysis buffer (89900, Thermo) supplemented with protease inhibitors (04693132001, Roche) and phosphatase inhibitor (4906837001, Roche) (for phosphoprotein detection). After centrifugation at 14,000 rpm for 10 minutes, the supernatants were collected and protein concentrations were determined using the Pierce BCA Protein Assay Kit (23225, Thermo Scientific) with bovine serum albumin as a protein standard. Proteins were separated by 10% SDS-PAGE and then transferred to a PVDF membrane. Membranes were blocked with 5% non-fat milk in TBST buffer (25 mM Tris pH 7.6, 150 mM NaCl, 2.5 mM KCl, 0.1% Triton-X100) for 1 hour and probed with primary antibodies overnight at 4 °C. After the membrane was washed with TBST three times, it was incubated with HRP-conjugated anti-rabbit or anti-mouse antibody for 1 hour at room temperature. The antibody information including species, source, catalog numbers and dilution is shown in Table S4. The target proteins were detected by enhanced chemiluminescence.

Please cite this article in press as: Zhang et al., Creatine promotes cancer metastasis through activation of Smad2/3, Cell Metabolism (2021), https://doi.org/10.1016/j.cmet.2021.03.009

Immunohistochemistry

Mouse tissues were fixed in 4% Paraformaldehyde solution overnight and then transferred to 70% ethanol for paraffin-embedded sections. Tissue sections were deparaffinized, rehydrated and boiled for 3 minutes in 10 mM pH 6 citrate buffer. Slides were blocked in 5% goat serum for 1 hour and then incubated at 4 °C overnight with anti-GATM, anti-Snail, and anti-Slug antibody. The antibody information is shown in Table S4. The following day, tissue sections were incubated with HRP-conjugated secondary antibody for 1 hour (6001, 6002, Zsbio), 3% hydrogen peroxide for 10 minutes and DAB for 1 minute (9019, Zsbio) followed by hematoxylin staining (9610, Zsbio). Sections were then dehydrated, mounted in neutral resins and analyzed using the Leica CS2 and Aperio ImageScope.

Cecum injection and mammary fat pad injection

In the cecum injection model, the mice were opened after anesthetization with isoflurane. Tumor cells were injected into the cecum wall, then the mice were closed using sterile suture. 2×10^6 HCT116 cells carrying mCherry or CRC57 cells carrying GFP vector were injected into NSG mice, while 1×10^5 CT26 cells carrying a luciferase vector were injected into BALB/c mice in the cecum injection model. In the mammary fat pad injection model, 5×10^5 4T1 cells were injected into BALB/c mice.

Human phosphorylation multi-pathway profiling array

Human phosphorylation multi-pathway profiling array C55 (AAH-PPP-1-2, RayBiotech) was used according to the manufacturer's instructions. Briefly, HCT116 cells were treated with or without creatine monohydrate (C3630, Sigma) in RPMI 1640 medium for 30 minutes. The cells were lysed using lysis buffer containing protease and phosphatase inhibitor cocktail. After the protein concentrations were measured using the Pierce BCA Protein Assay Kit, the same amount of cell lysates were incubated with the capture antibody-coaded array, followed by detection antibody cocktail and HRP-Anti-Rabbit IgG. The target proteins were detected by enhanced chemiluminescence. Gene Ontology (GO) analyses (Table S5) (R package "org.Hs.eg.db" and "clusterProfiler") were performed using the open source program R (version 3.5.1).

QUANTIFICATION AND STATISTICAL ANALYSIS

Quantification of metastasis

Mouse liver and lung tissues were fixed in 4% paraformaldehyde solution overnight and then transferred to 70% ethanol for paraffin-embedded sections. Paraffin-embedded liver and lung tissues were serially sectioned at 5 μm thickness. Ten sections of individual liver tissue and 5 sections of individual lung tissue taken at 100 μm thickness of the tissue were stained with hematoxylin and eosin (H&E). Metastatic nodules were qualified on the base of the H&E-stained sections. Luciferase signal was quantified using the IVIS luciferase imaging system lumina3.

Analysis of tissue microarray

Tissue microarrays ZL-HLin-Age075Met-01 (Zhuoli Biotechnology) and D1060401 (Bioaitech) were stained with anti-GATM (1:500, HPA026077) by the standard immunohistochemistry protocol descripted in this study. The patient information is shown in Table S2. Samples from 75% male and 25% female patients with age from 46 to 73 years old (mean age as 61) were included in tissue microarray ZL-HLin-Age075Met-01. Samples from 60% male and 40% female patients with age from 22 to 75 years old (mean age as 54) were included in tissue microarray D1060401. The stained tissue microarray was reviewed by a board-certified pathologist with experience in tumor biology without knowledge of the patient information of the tumor tissues. Each tissue core on the tissue microarray was given a score of 0–3 based on intensity of staining. Scores of 0 are interpreted as negative for protein expression while scores of 1, 2, and 3 are interpreted as positive staining for each tissue core.

Meta-analysis

Four NCBI: GEO datasets (Table S1) including clinical samples of primary CRC tumor and liver metastases were selected to investigate the differential transcriptomic signatures. Within these four datasets, a total of 58 paired, primary CRC tumor, and liver metastatic samples from 29 patients were integrated for analysis. The data were processed by quantile normalization and $\log_2$ transformation following the standard GEO2R analysis and then paired differential analysis were performed using the R package called Linear Models (Limma).

Statistical Analyses

Statistical analyses were performed with Graphpad Prism v.7 software. Sample normality was analyzed using D'Agostino & Pearson test and/or Shapiro–Wilk test. Comparisons between groups, whose distribution was determined as the normal distribution, were performed using two-tailed student's t-tests. Comparisons between groups, whose distribution could not been determined were performed using Mann-Whitney test. Survival curves were analyzed using log-rank test. The statistical analysis approaches were indicated in the figure legends. All graphs show mean ± SD or mean ± SEM as indicated in the figure legends. Limma was performed in Figures 2B and 2C, and Fisher's exact test was performed in Figure 4A as described in the correspondent figure legends. Each experiment was conducted with biological replicates and repeated no less than three times. Mice were randomly allocated to experimental groups.